

---

# PRE-TRAINING BY COMPLETING POINT CLOUDS

**Hanchen Wang**  
 University of Cambridge  
 hw501@cam.ac.uk

**Qi Liu**  
 University of Oxford  
 qiliu@cs.ox.ac.uk

**Xiangyu Yue**  
 UC Berkeley  
 xyyue@berkeley.edu

**Joan Lasenby**  
 University of Cambridge  
 jl221@cam.ac.uk

**Matt J. Kusner**  
 University College London  
 m.kusner@ucl.ac.uk

## ABSTRACT

There has recently been a flurry of exciting advances in deep learning models on point clouds. However, these advances have been hampered by the difficulty of creating labelled point cloud datasets: sparse point clouds often have unclear label identities for certain points, while dense point clouds are time-consuming to annotate. Inspired by mask-based pre-training in the natural language processing community, we propose a novel pre-training mechanism for point clouds. It works by masking occluded points that result from observing the point cloud at different camera views. It then optimizes a completion model that learns how to reconstruct the occluded points, given the partial point cloud. In this way, our method learns a pre-trained representation that can identify the visual constraints inherently embedded in real-world point clouds. We call our method *Occlusion Completion* (OcCo). We demonstrate that OcCo learns representations that improve generalization on downstream tasks over prior pre-training methods, that transfer to different datasets, that reduce training time, and improve labelled sample efficiency. Our code and dataset are available at <https://github.com/hansen7/OcCo>.

## 1 INTRODUCTION

Point clouds are a natural representation of 3D objects. They are crucial for various real-world applications in robotics (Yan et al., 2019), autonomous driving (Li, 2017; Yue et al., 2018), and localization (Elbaz et al., 2017; Angelina Uy & Hee Lee, 2018). Recently, there has been a flurry of exciting new point cloud models in areas such as segmentation (Landrieu & Simonovsky, 2018; Yang et al., 2019a; Hu et al., 2020a) and object detection (Zhou & Tuzel, 2018; Lang et al., 2019; Wang et al., 2020c). Current 3D sensing modalities (*i.e.*, 3D scanners, stereo cameras, lidars) have enabled the creation of large repositories of point cloud data (Rusu & Cousins, 2011; Hackel et al., 2017). However, annotating point clouds is challenging as: (1) Point cloud data can be sparse and at low resolutions, making the identity of points ambiguous; (2) Datasets that are not sparse can easily reach hundreds of millions of points (e.g., small dense point clouds for object classification (Zhou & Neumann, 2013) and large vast point clouds for 3D reconstruction (Zolanvari et al., 2019)); (3) Labelling individual points or drawing 3D bounding boxes are both more complex and time-consuming compared with annotating 2D images (Wang et al., 2019a). Since most methods require dense supervision, the lack of annotated point cloud data impedes the development of novel models.

On the other hand, because of the rapid development of 3D sensors, unlabelled point cloud datasets are abundant. Recent work has developed unsupervised pre-training methods to learn initialization for point cloud models. These are based on designing novel generative adversarial networks (GANs) (Wu et al., 2016; Han et al., 2019; Achlioptas et al., 2018) and autoencoders (Hassani & Haley, 2019; Li et al., 2018a; Yang et al., 2018). However, completely unsupervised pre-training methods have been recently outperformed by the self-supervised pre-training techniques of (Sauder & Sievers, 2019) and (Alliegro et al., 2020). Both methods work by first normalizing point clouds to the unit cube, then splitting each axis into  $k$  parts, yielding  $k^3$  voxels. Then, voxels are randomly permuted, and a model is trained to rearrange the permuted voxels back to their original positions. The intuition is that such a model learns the spatial configuration of objects and scenes. However, such random permutation

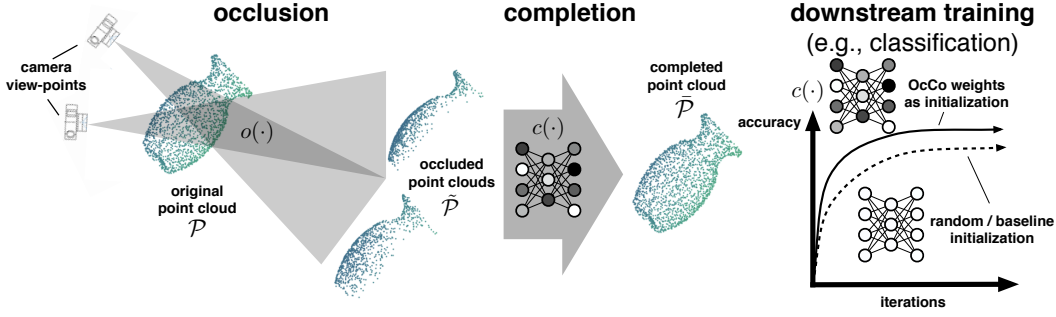


Figure 1: Occlusion Completion is a self-supervised pre-training method composed of two steps: (a) occlusion  $o(\cdot)$  of an input point cloud  $\mathcal{P}$  based on a random camera view-point into a partial point cloud  $\tilde{\mathcal{P}}$ , and (b) a model  $c(\cdot)$  that completes the occluded point cloud  $\tilde{\mathcal{P}}$  so that  $\tilde{\mathcal{P}} \approx \mathcal{P}$ . We demonstrate that the completion model  $c(\cdot)$  can be used as initialization for downstream tasks (e.g., classification, segmentation) leading to faster training and better generalization over existing methods.

destroys all spatial information that the model could have used to predict the final object point cloud. This potentially leads to prediction ambiguities: if two different objects have the same number of point cloud coordinates, then their random permutations are indistinguishable from each other.

Our insight is that partial point-cloud masking is a good candidate for pre-training in point-clouds because of two reasons: (1) The pre-trained model requires spatial and semantic understanding of the input point clouds to be able to reconstruct masked shapes. (2) Mask-based completion tasks have become the *de facto* standard for learning pre-trained representations in natural language processing (NLP) (Mikolov et al., 2013; Devlin et al., 2018; Peters et al., 2018). Different from random permutations, masking respects the spatial constraints that are naturally encoded in point clouds of real-world objects and scenes. Given this insight, we propose *Occlusion Completion* (OcCo) a novel pre-training method that consists of (a) a mechanism to generate occluded point clouds, and (b) a completion task to reconstruct the occluded point cloud.

Specifically, in (a) point clouds are generated by determining what part of objects would be occluded if the underlying object was observed from a particular view-point. In fact, many point clouds generated from a fixed 3D sensor will have occlusions exactly like this. Given an occluded point cloud, the goal of the completion task (b) is to learn a model that accurately reconstructs the missing parts of the point cloud. For a model to perform this task well, it needs to learn to encode localized structural information, based on the context and geometry of partial objects. This is something that is useful for any point cloud model to know, even if used only for classification or segmentation.

We demonstrate that the weights learned by our pre-training method *on a single unsupervised dataset* can be used as initialization for models in downstream tasks (e.g., object classification, part and semantic segmentation) to improve them, *even on completely different datasets*. Specifically our pre-training technique: (i) leads to improved generalization over prior baselines on the downstream tasks of object classification, object part and scene semantic segmentation; (ii) speeds up model convergence, in some cases, by up to  $5\times$ ; (iii) maintains improvements as the size of the labelled downstream dataset decreases; (iv) can be used for a variety of state-of-the-art point cloud models.

## 2 OCCLUSION COMPLETION

We now introduce Occlusion Completion. Our approach is shown in Figure 1. Our main insight is that by continually occluding point clouds and learning a model  $c(\cdot)$  to complete them, the weights of the completion model can be used as initialization for downstream tasks (e.g., classification, segmentation), speeding up training and improving generalization over other initialization techniques.

Throughout we will assume point clouds  $\mathcal{P}$  are sets of  $n$  points in 3D Euclidean space,  $\mathcal{P} = \{p_1, p_2, \dots, p_n\}$ , where each point  $p_i$  is a vector of coordinates  $(x_i, y_i, z_i)$  and extra features (e.g. color and normal vector). We begin by describing the components that make up our occlusion mapping  $o(\cdot)$ . We then detail how to learn a completion model  $c(\cdot)$ , giving pseudocode for the training task. Finally, we describe the architectural details we use to implement our approach.

---

## 2.1 GENERATING OCCLUSIONS

Our goal is to learn a randomized occlusion mapping  $o : \mathbb{P} \rightarrow \mathbb{P}$  (where  $\mathbb{P}$  is the space of all point clouds) from a full point cloud  $\mathcal{P}$  to an occluded point cloud  $\tilde{\mathcal{P}}$ . We will do so by determining which points are occluded when the point cloud is viewed from a particular camera position. This requires three steps: (1) A projection of the point cloud (in a world reference frame) into the coordinates of a camera reference frame; (2) Determining which points are occluded based on the camera view-points; (3) Mapping the points back from the camera reference frame to world reference frame.

**Viewing the point cloud from a camera.** A camera defines a projection from a 3D world reference frame into a distinctive 3D camera reference frame. It does so by specifying a camera model and a camera view-point from which the projection occurs. The simplest camera model is the pinhole camera, and view-point projection for it is given by a simple linear equation:

$$\begin{bmatrix} x_{\text{cam}} \\ y_{\text{cam}} \\ z_{\text{cam}} \end{bmatrix} = \underbrace{\begin{bmatrix} f & \gamma & w/2 \\ 0 & f & h/2 \\ 0 & 0 & 1 \end{bmatrix}}_{\text{intrinsic matrix } [\mathbf{K}]} \underbrace{\begin{bmatrix} r_1 & r_2 & r_3 & t_1 \\ r_4 & r_5 & r_6 & t_2 \\ r_7 & r_8 & r_9 & t_3 \end{bmatrix}}_{\text{rotation } [\mathbf{R}] \text{ | translation } [\mathbf{t}]} \begin{bmatrix} x \\ y \\ z \\ 1 \end{bmatrix}. \quad (1)$$

In the above,  $(x, y, z)$  are the original point cloud coordinates, the matrix including  $r$  and  $t$  entries is the concatenation of a 3D rotation matrix with a 3D translation vector, and the final matrix to the left is the camera intrinsic matrix ( $f$  specifies the camera focal length,  $\gamma$  is the skew between the  $x$  and  $y$  axes in the camera, and  $w, h$  are the width and height of the camera image). Given these, the final coordinates  $(x_{\text{cam}}, y_{\text{cam}}, z_{\text{cam}})$  are the positions of the point in the camera reference frame. We will refer to the intrinsic matrix as  $\mathbf{K}$  and the rotation/translation matrix as  $[\mathbf{R}|\mathbf{t}]$ .

**Determining occluded points.** We can think of the point  $(x_{\text{cam}}, y_{\text{cam}}, z_{\text{cam}})$  in multiple ways: (a) as a 3D point in the camera reference frame, (b) as a 2D pixel with coordinates  $(fx_{\text{cam}}/z_{\text{cam}}, fy_{\text{cam}}/z_{\text{cam}})$  with a depth of  $z_{\text{cam}}$ . In this way, some 2D points resulting from the projection may be occluded by others if they have the same pixel coordinates, but appear at a larger depth.

However, because point clouds only sparsely cover object surfaces, we need a way to (i) approximate the surface of the point cloud, and then (ii) determine which points are hidden by these surfaces. To approximate the surface (i) we create a polygon mesh of the camera reference point cloud (e.g., via Delaunay triangulation). Solving (ii) is referred to in computer graphics as the problem of *hidden-surface determination*. To solve this problem we use a well-known, highly-optimized technique called *z-buffering*. Z-buffering, also referred to as depth-buffering, works by continually estimating the minimum depth of each image pixel in the camera reference frame. It starts with an initial depth buffer of infinite distance for each pixel. Then by looping over each polygon faces of the 3D object, and each pixel in each polygon, z-buffering checks if the depth of that pixel is less than the depth in the buffer. If it is, it updates the depth buffer with the smaller depth. Thus, cloud points at a certain pixel are occluded if all surrounding polygons are at depths greater than the depth of that pixel in the final depth buffer. We remove all these occluded cloud points.

**Mapping back from camera frame to world frame.** Once occluded points are removed, we need to return the point cloud to the original world reference frame, via the following linear transformation:

$$\begin{bmatrix} x' \\ y' \\ z' \\ 1 \end{bmatrix} = \underbrace{\begin{bmatrix} r_1 & r_2 & r_3 & t_1 \\ r_4 & r_5 & r_6 & t_2 \\ r_7 & r_8 & r_9 & t_3 \\ 0 & 0 & 0 & 1 \end{bmatrix}^\top}_{\text{rotation } [\mathbf{R} | \mathbf{t}]^\top} \underbrace{\begin{bmatrix} 1/f & -\gamma/f^2 & (\gamma h - fw)/(2f^2) & 0 \\ 0 & 1/f & -h/(2f) & 0 \\ 0 & 0 & 1 & 0 \\ 0 & 0 & 0 & 1 \end{bmatrix}}_{\text{intrinsic inverse } [\mathbf{K}^{-1} | \mathbf{0}]} \begin{bmatrix} x_{\text{cam}} \\ y_{\text{cam}} \\ z_{\text{cam}} \\ 1 \end{bmatrix}. \quad (2)$$

Eq. (2) is the linear transformation that most closely approximates the inverse of eq. (1), producing point  $(x', y', z')$  in the world frame.

Thus, our randomized occlusion mapping  $o(\cdot)$  is constructed as follows. Fix an initial point cloud  $\mathcal{P}$ . Given a camera intrinsic matrix  $\mathbf{K}$ , sample rotation/translation matrices  $[[\mathbf{R}_1|\mathbf{t}_1], \dots, [\mathbf{R}_V|\mathbf{t}_V]]$ ,

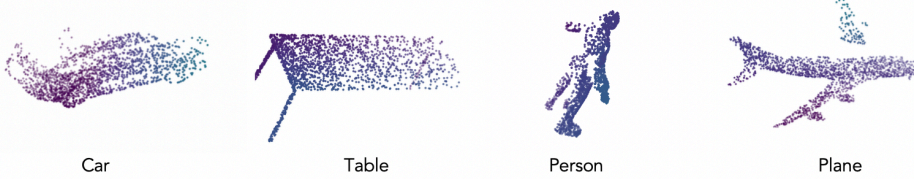


Figure 2: Examples of self-occluded objects generated by our method.

where  $V$  is the number of views. For each view  $v \in [V]$ , project  $\mathcal{P}$  into the camera frame of that view-point using eq. (1), find occluded points using z-buffering and remove them, then map the resulting point cloud back to the world reference frame using eq. (2). This yields the final occluded world frame point cloud for view-point  $v$ :  $\tilde{\mathcal{P}}_v$ .

## 2.2 THE COMPLETION TASK

Given an occluded point cloud  $\tilde{\mathcal{P}}$  produced by  $o(\cdot)$ , the goal of the completion task is to learn a completion mapping  $c : \mathbb{P} \rightarrow \mathbb{P}$  from  $\tilde{\mathcal{P}}$  to a completed point cloud  $\mathcal{P}$ . We say that a completion mapping is accurate w.r.t. loss  $\ell(\cdot, \cdot)$  if  $\mathbb{E}_{\tilde{\mathcal{P}} \sim o(\mathcal{P})} \ell(c(\tilde{\mathcal{P}}), \mathcal{P}) \rightarrow 0$ . The structure of the completion model  $c(\cdot)$  is an “encoder-decoder” style network (Dai et al., 2017b; Yuan et al., 2018; Tchapmi et al., 2019; Wang et al., 2020b). The encoder maps an occluded point cloud to a vector, and the decoder reconstructs the full point cloud. After pre-training, the encoder weights can be used as initialization for training downstream tasks. Algorithm 1 gives pseudocode for OcCo.

## 3 EXPERIMENTS

### 3.1 PRE-TRAINING AND DOWNSTREAM TRAINING DETAILS

**OcCo pre-training.** For all experiments, we will use a single pre-training dataset based on ModelNet40 (Wu et al., 2015). It includes 12,311 synthesized objects from 40 object categories, divided into 9,843 training objects and 2,468 testing objects. To construct the pre-training dataset, we generate occluded point clouds based on the training objects with a fixed camera intrinsics  $\{f = 1000, \gamma = 0, \omega = 1600, h = 1200\}$ , 10 random selected viewpoints and zero translation. Figure 2 shows examples of the resulting occluded point clouds. Note that these are qualitatively similar to point clouds in datasets where points are collected via 3D imaging devices such as handheld scanners (Dai et al., 2017a; Armeni et al., 2016) and lidar (Geiger et al., 2012). Given these, we use Algorithm 1 to train an “encoder-decoder” style completion model  $c(\cdot)$ . For encoders, similar to follow-up completion models (Tchapmi et al., 2019; Wang et al., 2020a; Wen et al., 2020), we consider PointNet (Qi et al., 2017a), Point Completion Network (PCN) (Yuan et al., 2018) and DGCNN (Wang et al., 2019b). These networks encode an occluded point cloud into a 1024-dimensional vector. We adapted the folding-based decoder from (Yuan et al., 2018) to complete the point clouds in a two-stage procedure. We use the Chamfer

---

### Algorithm 1 Occlusion Completion (OcCo)

---

```

# P: an initial point cloud
# K: camera intrinsic matrix
# V: number of total view points
# loss: a loss function between point clouds
# c: encoder-decoder completion model
# p: downstream prediction model

while i < V:
    # sample a random view-point
    R_t = [random.rotation(), random.translation()]

    # map point cloud to camera reference frame
    P_cam = dot(K, dot(R_t, P))

    # create occluded point cloud
    P_cam_oc = occlude(P_cam, alg='z-buffering')

    # point cloud back to world frame
    K_inv = [inv(K), zeros(3,1); zeros(1,3), 1]
    R_t_inv = transpose([R_t; zeros(3,1), 1])
    P_oc = dot(R_t_inv, dot(K_inv, P_cam_oc))

    # complete point cloud
    P_c = c.decoder(c.encoder(P_oc))

    # compute loss, update via gradient descent
    l = loss(P_c, P)
    l.backward()
    update(c.params)
    i += 1

# downstream tasks, use pre-trained encoders
p.initialize(c.encoder.params)
p.train()

```

---

Distance (CD) as our loss function  $\ell(\cdot, \cdot)$ . We use Adam (Kingma & Ba, 2015) with an initial learning rate of 1e-4, decayed by 0.7 every 20 epochs to a minimum value of 1e-6. We use a batch size of 32 and set the momentum in the batch normalisation to be 0.9.

Once we learn pre-trained OcCo weights on the ModelNet40, we will demonstrate the encoder weights improve initialization over prior baselines for downstream tasks: object classification, object part and scene semantic segmentation, *on any dataset*. This setup is challenging as the pre-training domain can be very different from the downstream domains. We detail the downstream tasks below.

**Object classification task.** For object classification we use six 3D object recognition benchmarks, we listed the descriptions in Table 1. All objects are represented with 1024 points. For PointNet and DGCNN baselines, we use the same training settings as the original literature, we adapt the output layers as well as the training setting for PCN based on those of PointNet (in appendix).

Table 1: Statistics of classification datasets

Name	Type	# Class	# Training	# Testing
ShapeNet10 (Chang et al., 2015)	synthesized	10	17,378	2,492
ModelNet40 (Wu et al., 2015)	synthesized	40	9,843	2,468
ShapeNet Oc (Yuan et al., 2018)	synthesized	8	231,792	800
ModelNet Oc (Our pre-training)	synthesized	40	98,430	24,680
ScanNet10 (Dai et al., 2017a)	real scanned	10	6,110	1,769
ScanObjectNN (Uy et al., 2019)	real scanned	15	2,304	576

**Part segmentation task.** We use the ShapeNetPart benchmark (Armeni et al., 2016) for object part segmentation. This dataset contains 16,881 objects from 16 categories, and has 50 parts in total. Each object is represented with 2048 points, and we use the same training settings as from the original literature. We also create the output layers for PCN encoder for this task (in appendix).

**Semantic segmentation task.** We use the S3DIS benchmark (Armeni et al., 2016) for semantic indoor scene segmentation. It contains 3D scans collected via Matterport scanners in 6 different places, encompassing 271 rooms. Each point, described by a 9-dimensional vector (including coordinates, RGB values and normalised location), is labeled as one of 13 semantic categories (e.g. chair, table and floor). We use the same preprocessing procedures and training settings as the original. In appendix, we describe how we modify the encoder and create the output layers for PCN.

### 3.2 COMPLETION RESULTS

In Figure 3, we first visualize the features learned by OcCo PointNet on the objects from test split of ModelNet40. We visualize each learned feature by coloring the points according to their channel values. We observe that, in early stage the encoder is able to learn low-level geometric primitives, i.e., planes, cylinders and cones, while later the network recognises more complex shapes like wings, leafs and upper bodies (non-rigid). We use t-SNE on the embeddings of OcCo-initialised encoders based on ShapeNet10, clearly separable clusters are formed for different object classes. We further train a linear SVM on these embeddings for classification and compare with prior works (in appendix).

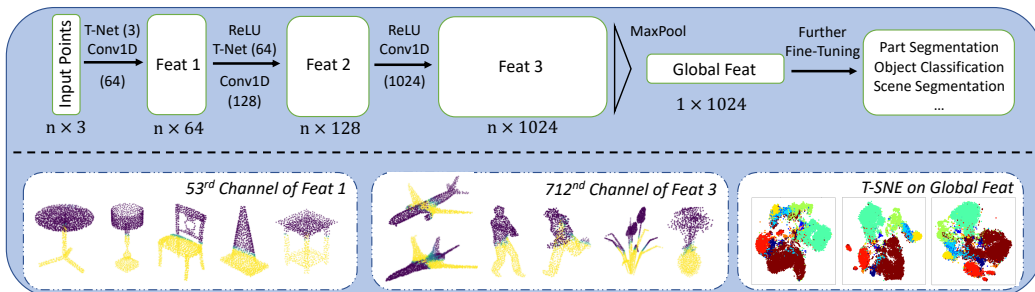


Figure 3: Interpretations on the learned features of OcCo-initialised encoders. Above half illustrates the location of learned features in the OcCo PointNet, below half interprets the learned features.

### 3.3 OBJECT CLASSIFICATION RESULTS

We now compare OcCo against prior initialization approaches on object classification tasks. Table 2 compares OcCo-initialization to random and (Sauder & Sievers, 2019)’s (Jigsaw) initialization on various object classification datasets among different encoders. We show that OcCo-initialized models outperform others in all cases. These results demonstrate that the OcCo-initialized models have strong transfer capabilities on out-of-domain datasets. We make more comparisons in the appendix.

Table 2: Comparison between OcCo, Jigsaw and Random (Rand) initialization on 3D object recognition benchmarks, based on PointNet, PCN and DGCNN encoders. Here “\*” marks the reported scores from the original literature (Qi et al., 2017a; Wang et al., 2019b; Uy et al., 2019; Sauder & Sievers, 2019) (we additionally confirm these scores are reproducible). Recall that OcCo-initialization is pre-trained only on occlusions generated from the train split of ModelNet40. We color **blue** the best results for each encoder and **bold** in black the overall best result for each dataset.

Dataset	PointNet			PCN			DGCNN		
	Rand	Jigsaw	OcCo	Rand	Jigsaw	OcCo	Rand	Jigsaw	OcCo
ShapeNet10	94.9	95.3	<b>95.5</b>	95.1	95.2	<b>95.4</b>	95.8	96.0	<b>96.6</b>
ModelNet40	89.2*	89.8	<b>90.2</b>	89.3	89.9	<b>90.5</b>	92.2*	92.4*	<b>93.1</b>
ShapeNet Oc	94.6	94.6	<b>95.0</b>	94.9	<b>95.1</b>	<b>95.1</b>	94.5	94.4	<b>95.1</b>
ModelNet Oc	85.3	85.5	<b>85.6</b>	84.6	<b>85.1</b>	<b>85.1</b>	88.7	88.7	<b>89.1</b>
ScanNet10	76.9	77.4	<b>78.2</b>	77.3	78.2	<b>78.4</b>	76.1	78.2	<b>78.8</b>
ScanObjectNN	73.7*	76.9	<b>80.2</b>	79.2	79.3	<b>80.6</b>	82.8*	83.2	<b>84.2</b>

### 3.4 OBJECT PART SEGMENTATION RESULTS

Table 3 compares OcCo-initialization to random and (Sauder & Sievers, 2019)’s (Jigsaw) initialization on object part segmentation task. We show that OcCo-initialized models outperform others in terms of accuracy and IoU in all three encoders, demonstrating representations derived from completing occluded ModelNet40 improves the performance of part segmentation (also by Figure 3).

Table 3: Overall point prediction accuracy (mAcc) and mean intersection of union (mIoU) on ShapeNetPart. As in Table 2, “\*” marks previously reported scores, and **blue** and **bold** are best scores.

	PointNet			PCN			DGCNN		
	Rand*	Jigsaw	OcCo	Rand	Jigsaw	OcCo	Rand*	Jigsaw*	OcCo
mAcc	93.2	93.6	<b>93.8</b>	92.9	93.0	<b>93.5</b>	93.2	94.1	<b>94.7</b>
mIoU	83.7	83.8	<b>84.4</b>	82.8	82.8	<b>83.7</b>	85.1	85.3	<b>85.5</b>

### 3.5 SEMANTIC SEGMENTATION

Here we compare random, Jigsaw and OcCo initialization on semantic segmentation task. We follow the same design of PointNet and DGCNN, use a  $k$ -fold train-test procedure as in (Armeni et al., 2016). The results are reported in Table 4. OcCo-initialized models outperform random and jigsaw-initialized ones, demonstrating that the pre-trained representations derived from completing occluded ModelNet40 brings improvements on segmenting indoor scenes which consist of occluded objects.<sup>1</sup>

Table 4: Overall point prediction accuracy (mAcc) and mean class intersection of union (mIoU) on the S3DIS averaged across 6-cv-fold. Again OcCo-initialized weights are pre-trained on ModelNet40.

	PointNet			PCN			DGCNN		
	Rand*	Jigsaw	OcCo	Rand	Jigsaw	OcCo	Rand*	Jigsaw	OcCo
mAcc	78.6	81.1	<b>82.6</b>	83.5	84.1	<b>85.6</b>	84.1	84.5	<b>84.9</b>
mIoU	47.7	53.8	<b>55.5</b>	52.5	53.3	<b>54.6</b>	56.1	56.4	<b>59.0</b>

<sup>1</sup>We noticed that the random initialised/pre-trained model in (Sauder & Sievers, 2019) (mIoU=40.3/41.2) did not achieve the similar results as the origin DGCNN (mIoU=56.1). They consider a transductive setting which is not directly comparable to ours, so here we stick to the supervised setting and report our reproduced scores.

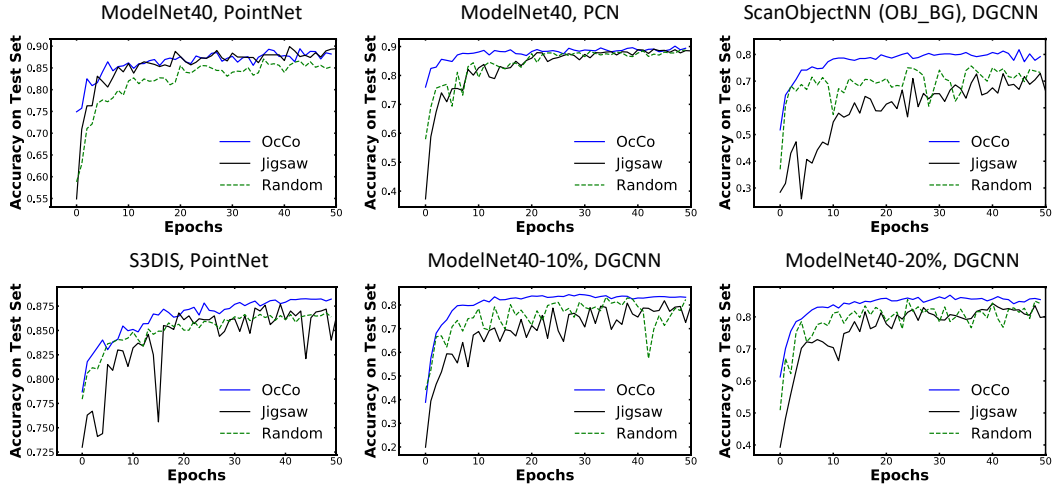


Figure 4: Learning curves of random, Jigsaw and OcCo initialised models on downstream tasks.

### 3.6 LABELLED SAMPLE EFFICIENCY

We investigate whether OcCo pre-training can improve the labelled sample efficiency of downstream tasks. Specifically, we reduce the labelled samples to 1%, 5%, 10% and 20% of the original training set for the ModelNet40 object classification task, and evaluate on the full test set. As shown in Table 5, OcCo-initialized models achieve superior results compared to the randomly-initialized models, demonstrating that OcCo with in-domain pre-training improves labelled sample efficiency.

Table 5: Sample efficiency with randomly-initialized and OcCo-initialized models.

Baseline	PointNet			PCN			DGCNN		
	Rand	Jigsaw	OcCo	Rand	Jigsaw	OcCo	Rand	Jigsaw	OcCo
1%	56.9	55.7	<b>58.1</b>	57.8	59.6	<b>60.4</b>	60.0	59.9	<b>60.5</b>
5%	73.9	74.3	<b>74.9</b>	73.2	75.8	<b>76.7</b>	79.4	79.2	<b>79.7</b>
10%	80.6	<b>81.3</b>	81.1	81.1	82.1	<b>82.6</b>	84.4	84.4	<b>84.5</b>
20%	83.6	<b>84.2</b>	<b>84.2</b>	83.6	84.2	<b>84.4</b>	86.5	86.7	<b>87.2</b>

### 3.7 LEARNING CURVES

We plot the learning curves for classification and segmentation tasks in Figure 4. We observe that the models with OcCo initialization converge faster to better test accuracy than the random and sometimes Jigsaw-initialized models. For example, on ModelNet40 with a PCN encoder, the OcCo-initialized model takes around 10 epochs to converge, while the randomly initialized model takes around 50 epochs. Similarly, for ScanObjectNN (OBJ\_BG) with DGCNN encoder, the OcCo-initialized model converges around 20 epochs and to a better test accuracy than the random-initialized model.

## 4 RELATED WORK

### 4.1 DEEP MODELS FOR POINT CLOUDS

Work on deep models for point clouds can largely be divided into three different structural approaches: (a) *pointwise-based networks*, (b) *convolution-based networks*, and (c) *graph-based networks*. We call the networks that independently process each point, before aggregating these point representations: *pointwise-based networks* (Qi et al., 2017a;b; Joseph-Rivlin et al., 2019; Duan et al., 2019; Zhao et al., 2019; Yang et al., 2019b; Lin et al., 2019). One well-known method, PointNet, devises a novel neural network that is designed to respect the permutation invariance of point clouds. Each point is independently fed into a multi-layer perceptron, then outputs are aggregated using a permutation-invariant function (e.g., max-pooling) to obtain a global point cloud representation. Another class of methods are *convolution-based networks* (Hua et al., 2018; Su et al., 2018; Li et al., 2018b; Atzmon et al., 2018; Landrieu & Simonovsky, 2018; Hermosilla et al., 2018; Groh et al., 2018; Rao et al., 2019). These works map point clouds to regular grid structures and extend the classic convolution operator to handle these grid structures. A representative model, PCNN (Atzmon et al., 2018), defines

---

two operators, extension and restriction, for mapping point cloud functions to volumetric functions and vice versa. The third class of models is *graph-based networks* (Simonovsky & Komodakis, 2017; Wang et al., 2019b; Shen et al., 2018; Wang et al., 2018; Zhang & Rabbat, 2018; Chen et al., 2019). These networks regard each point as a vertex of a graph and generate edges based on spatial information and node similarities. A popular method is DGCNN (Wang et al., 2019b), which introduces a new operation, EdgeConv, to aggregate local features and a graph update module to learn dynamic graph relations from layer to layer. NRS (Cao et al., 2020) uses a neural random subspace method based on the encoded embeddings to further improve the performance of the models.

## 4.2 PRE-TRAINING FOR POINT CLOUDS

Pre-training models on unlabelled data are gaining popularity recently due to its success on a wide range of tasks, such as natural language understanding (Mikolov et al., 2013; Devlin et al., 2018), object detection (He et al., 2020; Chen et al., 2020) and graph representations (Hu et al., 2020b;c). The representations learned from these pre-trained models can be used as a good initializer in downstream tasks, where task-specific annotated samples are scarce. Three types of pre-training objectives are adopted for point clouds, based on: generative adversarial networks (GAN), autoencoders, and spatial relation reconstruction (Sauder & Sievers, 2019). However, GANs for point clouds are limited to non-point-set inputs, i.e., voxelized representations (Wu et al., 2016), 2D depth images of point clouds (Han et al., 2019), and latent representations from autoencoders (Achlioptas et al., 2018), as sampling point sets from a neural network is non-trivial. Thus these GAN approaches cannot leverage the natural order-invariance of point-sets. Autoencoders for point clouds (Yang et al., 2018; Li et al., 2018a; Hassani & Haley, 2019; Shi et al., 2020) learn to encode point clouds into a latent space before reconstructing these point clouds from their latent representation. Yet, there is recent evidence that the representations learned by autoencoders are not necessarily good when used as initialization for downstream tasks (Alberti et al., 2017). In fact, both GAN and autoencoder-based pre-training methods have been recently outperformed on downstream tasks by the pre-training technique of (Sauder & Sievers, 2019).

These methods are based on spatial relation reconstruction, which aims to reconstruct points clouds given rearranged point clouds as input. To this end, Sauder & Sievers (2019) equally split the 3D space into  $k^3$  voxels, rearrange  $k^3$  voxels and train a model to predict the original voxel label for each point. (Alliegro et al., 2020) further developed this approach into a multi-task learning framework where other tasks are supervised, i.e. classification and part segmentation. However, these random permutations destroy all spatial information that the model could have used to predict the true point cloud. Instead, our method creates spatially realistic occlusions that a completion model learns to reconstruct. As such, this model learns how to naturally encode 3D object shape and contextual information. There is a new method called PointContrast (Xie et al., 2020) which mainly uses contrastive learning for pre-training point cloud segmentation models. Our method is more general and transferable compared with theirs.

## 5 DISCUSSION

In this work, we have demonstrated that Occlusion Completion (OcCo) learns generalizable representations for a variety of point cloud learning tasks, while increasing labelled sample efficiency and model convergence speed. There are a few exciting directions that we would like to explore in future. First, we believe this method would be useful as a data-augmentation technique during training to improve robustness, similar to input dropout in the 2D case Bouthillier et al. (2015). Second, it would be interesting to design a completion model that is explicitly aware that it is completing an occluded view-point. A model like this would likely converge even quicker, and require fewer parameters, as this knowledge could act as a stronger inductive bias during learning. In general, we advocate for structuring deep models using graphical constraints as an inductive bias to improve learning.

## Acknowledgments

---

## REFERENCES

Panos Achlioptas, Olga Diamanti, Ioannis Mitliagkas, and Leonidas J. Guibas. Learning representations and generative models for 3d point clouds. In *International Conference on Machine Learning (ICML)*, 2018.

Michele Alberti, Mathias Seuret, Rolf Ingold, and Marcus Liwicki. A pitfall of unsupervised pre-training. *arXiv preprint arXiv:1703.04332*, 2017.

Antonio Alliegro, Davide Boscaini, and Tatiana Tommasi. Joint supervised and self-supervised learning for 3d real-world challenges. *arXiv preprint arXiv:2004.07392*, 2020.

Mikaela Angelina Uy and Gim Hee Lee. Pointnetvlad: Deep point cloud based retrieval for large-scale place recognition. In *The IEEE Conference on Computer Vision and Pattern Recognition (CVPR)*, 2018.

Iro Armeni, Ozan Sener, Amir R Zamir, Helen Jiang, Ioannis Brilakis, Martin Fischer, and Silvio Savarese. 3d semantic parsing of large-scale indoor spaces. In *The IEEE Conference on Computer Vision and Pattern Recognition (CVPR)*, 2016.

Matan Atzmon, Haggai Maron, and Yaron Lipman. Point convolutional neural networks by extension operators. *ACM Transactions on Graphics (TOG)*, 37(4):71:1–71:12, 2018.

Dimitri P Bertsekas. A distributed asynchronous relaxation algorithm for the assignment problem. In *The IEEE Conference on Decision and Control*, 1985.

Xavier Bouthillier, Kishore Konda, Pascal Vincent, and Roland Memisevic. Dropout as data augmentation. *arXiv preprint arXiv:1506.08700*, 2015.

Yun-Hao Cao, Jianxin Wu, Hanchen Wang, and Joan Lasenby. Neural random subspace. *arXiv preprint arXiv:1911.07845*, 2020.

Angel X Chang, Thomas Funkhouser, Leonidas Guibas, Pat Hanrahan, Qixing Huang, Zimo Li, Silvio Savarese, Manolis Savva, Shuran Song, Hao Su, et al. Shapenet: An information-rich 3d model repository. *arXiv preprint arXiv:1512.03012*, 2015.

Chao Chen, Guanbin Li, Ruijia Xu, Tianshui Chen, Meng Wang, and Liang Lin. Clusternet: Deep hierarchical cluster network with rigorously rotation-invariant representation for point cloud analysis. In *The IEEE Conference on Computer Vision and Pattern Recognition (CVPR)*, 2019.

Ting Chen, Simon Kornblith, Mohammad Norouzi, and Geoffrey Hinton. A simple framework for contrastive learning of visual representations. *International Conference on Machine Learning (ICML)*, 2020.

Angela Dai, Angel X. Chang, Manolis Savva, Maciej Halber, Thomas Funkhouser, and Matthias Nießner. Scannet: Richly-annotated 3d reconstructions of indoor scenes. In *Proc. Computer Vision and Pattern Recognition (CVPR), IEEE*, 2017a.

Angela Dai, Charles Ruizhongtai Qi, and Matthias Nießner. Shape completion using 3d-encoder-predictor cnns and shape synthesis. In *The IEEE Conference on Computer Vision and Pattern Recognition (CVPR)*, 2017b.

Jacob Devlin, Ming-Wei Chang, Kenton Lee, and Kristina Toutanova. Bert: Pre-training of deep bidirectional transformers for language understanding. *arXiv preprint arXiv:1810.04805*, 2018.

Yueqi Duan, Yu Zheng, Jiwen Lu, Jie Zhou, and Qi Tian. Structural relational reasoning of point clouds. In *The IEEE Conference on Computer Vision and Pattern Recognition (CVPR)*, 2019.

Gil Elbaz, Tamar Avraham, and Anath Fischer. 3d point cloud registration for localization using a deep neural network auto-encoder. In *The IEEE Conference on Computer Vision and Pattern Recognition (CVPR)*, 2017.

Andreas Geiger, Philip Lenz, and Raquel Urtasun. Are we ready for autonomous driving? the kitti vision benchmark suite. In *The IEEE Conference on Computer Vision and Pattern Recognition (CVPR)*, 2012.

---

Fabian Groh, Patrick Wieschollek, and Hendrik Lensch. Flex-convolution (million-scale point-cloud learning beyond grid-worlds). *arXiv preprint arXiv:1803.07289*, 2018.

Daniel Guo, Bernardo Ávila Pires, Bilal Piot, Jean-Bastien Grill, Florent Altché, Rémi Munos, and Mohammad Gheshlaghi Azar. Bootstrap latent-predictive representations for multitask reinforcement learning. In *International Conference on Machine Learning (ICML)*, 2020.

Timo Hackel, N. Savinov, L. Ladicky, Jan D. Wegner, K. Schindler, and M. Pollefeys. SEMANTIC3D.NET: A new large-scale point cloud classification benchmark. In *ISPRS Annals of the Photogrammetry, Remote Sensing and Spatial Information Sciences*, volume IV-1-W1, pp. 91–98, 2017.

Zhizhong Han, Mingyang Shang, Yu-Shen Liu, and Matthias Zwicker. View inter-prediction gan: Unsupervised representation learning for 3d shapes by learning global shape memories to support local view predictions. In *Proceedings of the AAAI Conference on Artificial Intelligence*, 2019.

Kaveh Hassani and Mike Haley. Unsupervised multi-task feature learning on point clouds. In *The IEEE International Conference on Computer Vision (CVPR)*, 2019.

Kaiming He, Haoqi Fan, Yuxin Wu, Saining Xie, and Ross Girshick. Momentum contrast for unsupervised visual representation learning. *The IEEE Conference on Computer Vision and Pattern Recognition (CVPR)*, 2020.

Pedro Hermosilla, Tobias Ritschel, Pere-Pau Vázquez, Àlvar Vinacua, and Timo Ropinski. Monte carlo convolution for learning on non-uniformly sampled point clouds. *ACM Transactions on Graphics (TOG)*, 37(6):1–12, 2018.

Qingyong Hu, Bo Yang, Linhai Xie, Stefano Rosa, Yulan Guo, Zhihua Wang, Niki Trigoni, and Andrew Markham. Randla-net: Efficient semantic segmentation of large-scale point clouds. *Proceedings of the IEEE Conference on Computer Vision and Pattern Recognition (CVPR)*, 2020a.

Weihua Hu, Bowen Liu, Joseph Gomes, Marinka Zitnik, Percy Liang, Vijay Pande, and Jure Leskovec. Strategies for pre-training graph neural networks. In *International Conference on Learning Representations (ICLR)*, 2020b.

Ziniu Hu, Yuxiao Dong, Kuansan Wang, Kai-Wei Chang, and Yizhou Sun. Gpt-gnn: Generative pre-training of graph neural networks. In *Proceedings of the 26th ACM SIGKDD International Conference on Knowledge Discovery and Data Mining (KDD)*, 2020c.

Binh-Son Hua, Minh-Khoi Tran, and Sai-Kit Yeung. Pointwise convolutional neural networks. In *The IEEE Conference on Computer Vision and Pattern Recognition (CVPR)*, 2018.

Mor Joseph-Rivlin, Alon Zvirin, and Ron Kimmel. Momen (e) t: Flavor the moments in learning to classify shapes. In *The IEEE International Conference on Computer Vision Workshops (CVPRW)*, 2019.

Diederik P. Kingma and Jimmy Ba. Adam: A method for stochastic optimization. In *International Conference on Learning Representations (ICLR)*, 2015.

Loic Landrieu and Martin Simonovsky. Large-scale point cloud semantic segmentation with superpoint graphs. In *The IEEE Conference on Computer Vision and Pattern Recognition (CVPR)*, 2018.

Alex H Lang, Sourabh Vora, Holger Caesar, Lubing Zhou, Jiong Yang, and Oscar Beijbom. Pointpillars: Fast encoders for object detection from point clouds. In *The IEEE Conference on Computer Vision and Pattern Recognition (CVPR)*, 2019.

Bo Li. 3d fully convolutional network for vehicle detection in point cloud. In *The IEEE/RSJ International Conference on Intelligent Robots and Systems (IROS)*, 2017.

Jiaxin Li, Ben M Chen, and Gim Hee Lee. So-net: Self-organizing network for point cloud analysis. In *The IEEE conference on computer vision and pattern recognition (CVPR)*, 2018a.

---

Yangyan Li, Rui Bu, Mingchao Sun, and Baoquan Chen. Pointcnn. *Advances in neural information processing systems (NeurIPS)*, 2018b.

Hongxin Lin, Zelin Xiao, Yang Tan, Hongyang Chao, and Shengyong Ding. Justlookup: One millisecond deep feature extraction for point clouds by lookup tables. In *The IEEE International Conference on Multimedia and Expo (ICME)*, 2019.

Tomas Mikolov, Kai Chen, Greg Corrado, and Jeffrey Dean. Efficient estimation of word representations in vector space. *arXiv preprint arXiv:1301.3781*, 2013.

Matthew E. Peters, Mark Neumann, Mohit Iyyer, Matt Gardner, Christopher Clark, Kenton Lee, and Luke Zettlemoyer. Deep contextualized word representations. In *The North American Chapter of the Association for Computational Linguistics: Human Language Technologies, (NAACL-HLT)*, 2018.

Charles R Qi, Hao Su, Kaichun Mo, and Leonidas J Guibas. Pointnet: Deep learning on point sets for 3d classification and segmentation. In *The IEEE conference on computer vision and pattern recognition (CVPR)*, 2017a.

Charles Ruizhongtai Qi, Li Yi, Hao Su, and Leonidas J Guibas. Pointnet++: Deep hierarchical feature learning on point sets in a metric space. In *Advances in neural information processing systems (NeurIPS)*, 2017b.

Yongming Rao, Jiwen Lu, and Jie Zhou. Spherical fractal convolutional neural networks for point cloud recognition. In *The IEEE Conference on Computer Vision and Pattern Recognition (CVPR)*, 2019.

Radu Bogdan Rusu and Steve Cousins. 3D is here: Point Cloud Library (PCL). In *The IEEE International Conference on Robotics and Automation (ICRA)*, 2011.

Jonathan Sauder and Bjarne Sievers. Self-supervised deep learning on point clouds by reconstructing space. In *Advances in Neural Information Processing Systems (NeurIPS)*, 2019.

Yiru Shen, Chen Feng, Yaoqing Yang, and Dong Tian. Mining point cloud local structures by kernel correlation and graph pooling. In *The IEEE conference on computer vision and pattern recognition (CVPR)*, 2018.

Yi Shi, Mengchen Xu, Shuaihang Yuan, and Yi Fang. Unsupervised deep shape descriptor with point distribution learning. In *The IEEE Conference on Computer Vision and Pattern Recognition (CVPR)*, 2020.

Martin Simonovsky and Nikos Komodakis. Dynamic edge-conditioned filters in convolutional neural networks on graphs. In *The IEEE conference on computer vision and pattern recognition (CVPR)*, 2017.

Hang Su, Varun Jampani, Deqing Sun, Subhransu Maji, Evangelos Kalogerakis, Ming-Hsuan Yang, and Jan Kautz. Splatnet: Sparse lattice networks for point cloud processing. In *The IEEE Conference on Computer Vision and Pattern Recognition (CVPR)*, 2018.

Lyne P. Tchapmi, Vineet Kosaraju, Hamid Rezatofighi, Ian Reid, and Silvio Savarese. Topnet: Structural point cloud decoder. In *The IEEE Conference on Computer Vision and Pattern Recognition (CVPR)*, 2019.

Mikaela Angelina Uy, Quang-Hieu Pham, Binh-Son Hua, Thanh Nguyen, and Sai-Kit Yeung. Revisiting point cloud classification: A new benchmark dataset and classification model on real-world data. In *IEEE International Conference on Computer Vision (ICCV)*, 2019.

Bernie Wang, Virginia Wu, Bichen Wu, and Kurt Keutzer. Latte: accelerating lidar point cloud annotation via sensor fusion, one-click annotation, and tracking. In *The IEEE Intelligent Transportation Systems Conference (ITSC)*, 2019a.

Chu Wang, Babak Samari, and Kaleem Siddiqi. Local spectral graph convolution for point set feature learning. In *European conference on computer vision (ECCV)*, 2018.

---

Xiaogang Wang, Marcelo H. Ang, and Gim Hee Lee. Cascaded refinement network for point cloud completion. In *The IEEE Conference on Computer Vision and Pattern Recognition (CVPR)*, 2020a.

Xiaogang Wang, Marcelo H. Ang Jr., and Gim Hee Lee. Cascaded refinement network for point cloud completion. In *The IEEE Conference on Computer Vision and Pattern Recognition (CVPR)*, 2020b.

Yue Wang, Yongbin Sun, Ziwei Liu, Sanjay E Sarma, Michael M Bronstein, and Justin M Solomon. Dynamic graph cnn for learning on point clouds. *ACM Transactions on Graphics (TOG)*, 38(5):1–12, 2019b.

Yue Wang, Alireza Fathi, Abhijit Kundu, David Ross, Caroline Pantofaru, Tom Funkhouser, and Justin Solomon. Pillar-based object detection for autonomous driving. In *European Conference on Computer Vision (ECCV)*, 2020c.

Xin Wen, Tianyang Li, Zhizhong Han, and Yu-Shen Liu. Point cloud completion by skip-attention network with hierarchical folding. In *The IEEE Conference on Computer Vision and Pattern Recognition (CVPR)*, 2020.

Jiajun Wu, Chengkai Zhang, Tianfan Xue, Bill Freeman, and Josh Tenenbaum. Learning a probabilistic latent space of object shapes via 3d generative-adversarial modeling. In *Advances in neural information processing systems (NeurIPS)*, 2016.

Zhirong Wu, Shuran Song, Aditya Khosla, Fisher Yu, Linguang Zhang, Xiaou Tang, and Jianxiong Xiao. 3d shapenets: A deep representation for volumetric shapes. In *the IEEE conference on computer vision and pattern recognition (CVPR)*, 2015.

Saining Xie, Jiatao Gu, Demi Guo, Charles R Qi, Leonidas J Guibas, and Or Litany. Pointcontrast: Unsupervised pre-training for 3d point cloud understanding. In *European conference on computer vision (ECCV)*, 2020.

Xinchen Yan, Mohi Khansari, Jasmine Hsu, Yuanzheng Gong, Yunfei Bai, Sören Pirk, and Honglak Lee. Data-efficient learning for sim-to-real robotic grasping using deep point cloud prediction networks. *arXiv preprint arXiv:1906.08989*, 2019.

Bo Yang, Jianan Wang, Ronald Clark, Qingyong Hu, Sen Wang, Andrew Markham, and Niki Trigoni. Learning object bounding boxes for 3d instance segmentation on point clouds. In *Advances in Neural Information Processing Systems (NeurIPS)*, 2019a.

Jiancheng Yang, Qiang Zhang, Bingbing Ni, Linguo Li, Jinxian Liu, Mengdie Zhou, and Qi Tian. Modeling point clouds with self-attention and gumbel subset sampling. In *The IEEE Conference on Computer Vision and Pattern Recognition (CVPR)*, 2019b.

Yaoqing Yang, Chen Feng, Yiru Shen, and Dong Tian. Foldingnet: Point cloud auto-encoder via deep grid deformation. In *Proceedings of the IEEE Conference on Computer Vision and Pattern Recognition*, pp. 206–215, 2018.

Wentao Yuan, Tejas Khot, David Held, Christoph Mertz, and Martial Hebert. Pcn: Point completion network. In *2018 International Conference on 3D Vision (3DV)*, pp. 728–737. IEEE, 2018.

Xiangyu Yue, Bichen Wu, Sanjit A Seshia, Kurt Keutzer, and Alberto L Sangiovanni-Vincentelli. A lidar point cloud generator: from a virtual world to autonomous driving. In *Proceedings on International Conference on Multimedia Retrieval*, pp. 458–464, 2018.

Yingxue Zhang and Michael Rabbat. A graph-cnn for 3d point cloud classification. In *The IEEE International Conference on Acoustics, Speech and Signal Processing (ICASSP)*, 2018.

Hengshuang Zhao, Li Jiang, Chi-Wing Fu, and Jiaya Jia. Pointweb: Enhancing local neighborhood features for point cloud processing. In *The IEEE Conference on Computer Vision and Pattern Recognition (CVPR)*, 2019.

Qian-Yi Zhou and Ulrich Neumann. Complete residential urban area reconstruction from dense aerial lidar point clouds. *Graphical Models*, 75(3):118–125, 2013.

---

Yin Zhou and Oncel Tuzel. Voxelnet: End-to-end learning for point cloud based 3d object detection. In *The IEEE Conference on Computer Vision and Pattern Recognition (CVPR)*, 2018.

SM Zolanvari, Susana Ruano, Aakanksha Rana, Alan Cummins, Rogerio Eduardo da Silva, Morteza Rahbar, and Aljosa Smolic. Dublincity: Annotated lidar point cloud and its applications. In *British Machine Vision Conference (BMVC)*, 2019.

---

## A DESIGN OF THE COMPLETION MODEL

Previous point completion models (Dai et al., 2017b; Yuan et al., 2018; Tchapmi et al., 2019; Wang et al., 2020b) all use an "encoder-decoder" architecture. The encoder maps a partial point cloud to a vector of a fixed dimension, and the decoder reconstructs the full point cloud.

In the OcCo experiments, we exclude the last few MLPs of PointNet and DGCNN, and use the remaining architecture as the encoder to map a partial point cloud into a 1024-dimensional vector. We adapt the folding-based decoder design from PCN, which is a two-stage point cloud generator that produces a coarse and a fine-grained output point cloud ( $Y_{coarse}, Y_{fine}$ ) for each input. We removed all the batch normalisation layers in the folding-based decoder since we find it brings negative effects in the completion process in terms of Chamfer distance loss and convergent speed. On the basis of prior self-supervised learning methods, SimCLR (Chen et al., 2020), MoCo (He et al., 2020) and BYOL (Guo et al., 2020), we find the batch normalisation is important in the encoder yet harmful for the encoder. Also, we find the L2 normalisation in the Adam optimiser is undesired for completion training but brings improvements on the downstream fine-tuning.

The predicted coarse point cloud  $\hat{Y}_{coarse}$ , which represents the global geometry of a shape, is generated via a set of fully connected layers. A folding-based generator is used to predict the local fine structures of each point in  $\hat{Y}_{coarse}$ , this results in  $\hat{Y}_{fine}$ . The folding based structures is proved to be good at approximating a smooth surface which reflects the local geometry. During training,  $Y_{coarse}$  and  $Y_{fine}$  are generated via randomly sampling 1024 and 16384 points from the mesh, respectively.

We use either Chamfer Distance (CD) or Earth Mover Distance (EMD) as the loss function for the completion model. We use a normalised and symmetric (thus commutative) version of Chamfer Distance (CD) to quantify the differences between two point clouds  $\hat{P}$  and  $P$ :

$$CD(\hat{P}, P) = \frac{1}{|\hat{P}|} \sum_{\hat{x} \in \hat{P}} \min_{x \in P} \| \hat{x} - x \|_2 + \frac{1}{|P|} \sum_{x \in P} \min_{\hat{x} \in \hat{P}} \| x - \hat{x} \|_2. \quad (3)$$

Note that it is no need that the two point cloud  $\hat{P}$  and  $P$  have the same size. But when calculating the Earth Mover Distance (EMD),  $\hat{P}$  and  $P$  are usually required to have same number of points:

$$EMD(\hat{P}, P) = \min_{\phi: \hat{P} \rightarrow P} \frac{1}{|\hat{P}|} \sum_{\hat{x} \in \hat{P}} \| \hat{x} - \phi(\hat{x}) \|_2, \quad (4)$$

where  $\phi$  is a bijection between points in  $\hat{P}$  and  $P$ . Note that EMD is not commutative. Since finding the optimal mapping  $\phi$  is quite time consuming, we use its approximation form Bertsekas (1985).

The loss  $l$  of the completion task is a adaptive weighted sum of coarse and fine generations:

$$l = d_1(\hat{Y}_{coarse}, Y_{coarse}) + \alpha * d_2(\hat{Y}_{fine}, Y_{fine}), \quad (5)$$

where the step-wise trade-off coefficient  $\alpha$  incrementally grows during training. In our experiments, we find that even with approximation, it is still suboptimal to use EMD for  $d_2$ , since it is inefficient to solve the approximate bijection mapping  $\phi$  for over 16k point pairs. We evaluate both 'EMD+CD' and 'CD+CD' combinations for the loss  $l$ . We have found that OcCo with 'EMD+CD' loss has achieved comparable performance yet longer time in the downstream classification tasks compared with the 'CD+CD'. We use 'CD+CD' as the loss function in the OcCo pre-training process described in Section. 3.1 in terms of simplicity and efficiency.

## B QUALITATIVE RESULTS FROM OCCO PRE-TRAINING

In this section, we show some qualitative results of OcCo pre-training by visualising the input, coarse output, fine output and ground truth at different training epochs and encoders. In Figure. 5, Figure. 6 and Figure. 7, we notice that the trained completion models are able to complete even difficult occluded shapes such as plants and planes. In Figure. 8 we plot some failure examples of completed shapes, possibly due to their complicated fine structures, while it is worth mentioning that the completed model can still completed these objects under the same category.

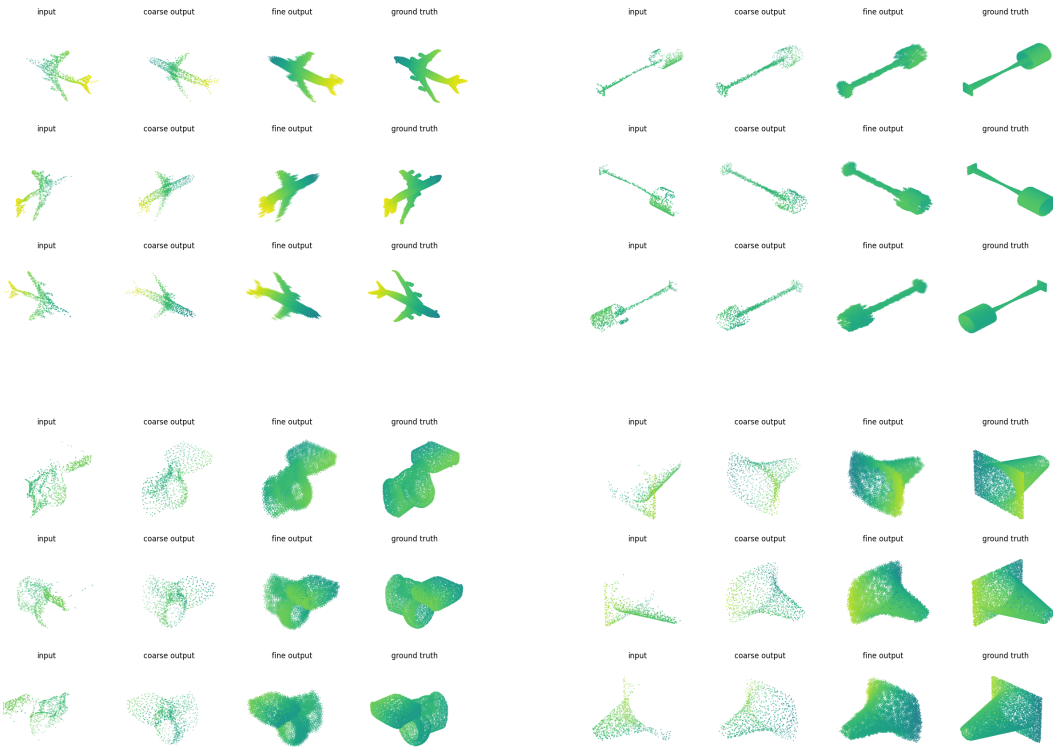


Figure 5: OcCo pre-training with PCN encoder on occluded ModelNet40.

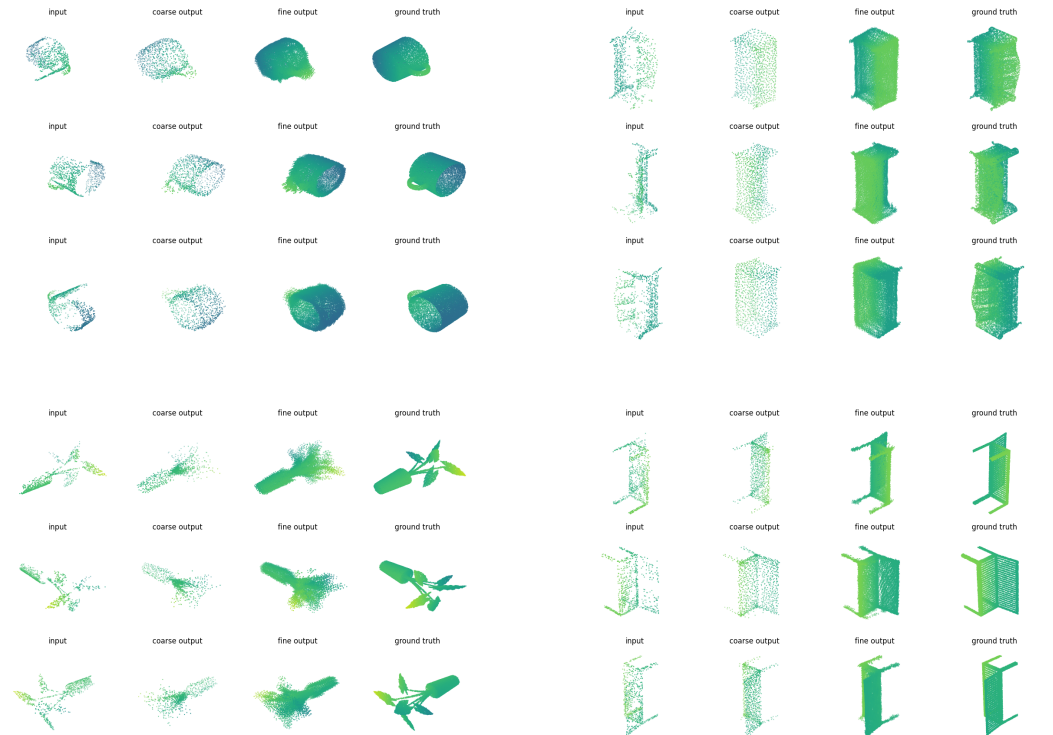


Figure 6: OcCo pre-training with PointNet encoder on occluded ModelNet40.

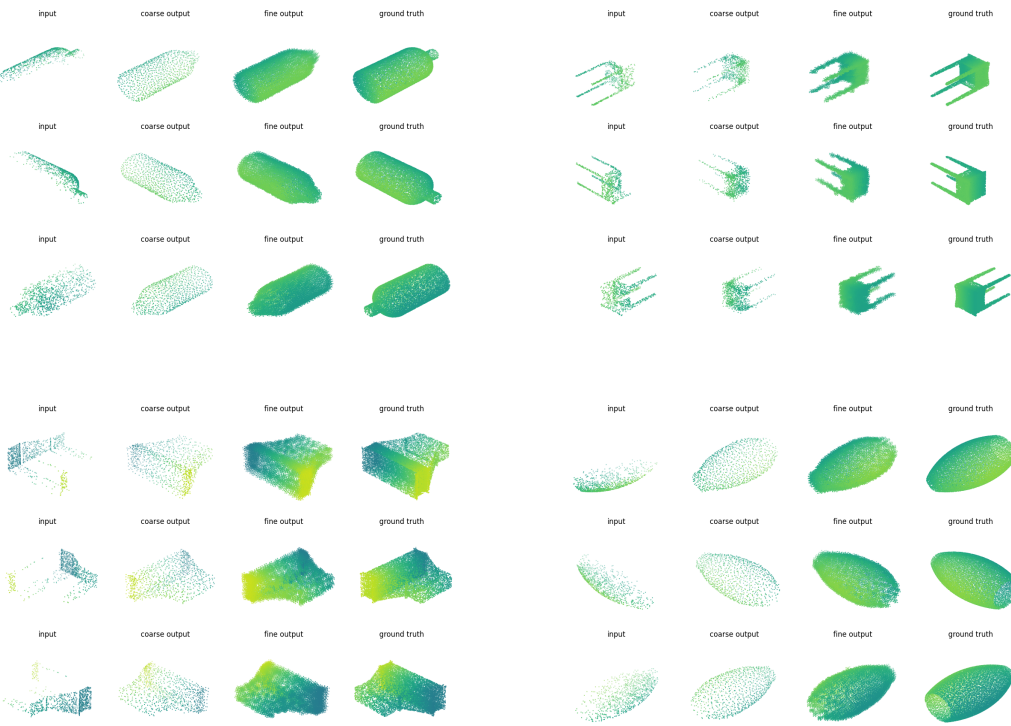


Figure 7: OcCo pre-training with DGCNN encoder on occluded ModelNet40.

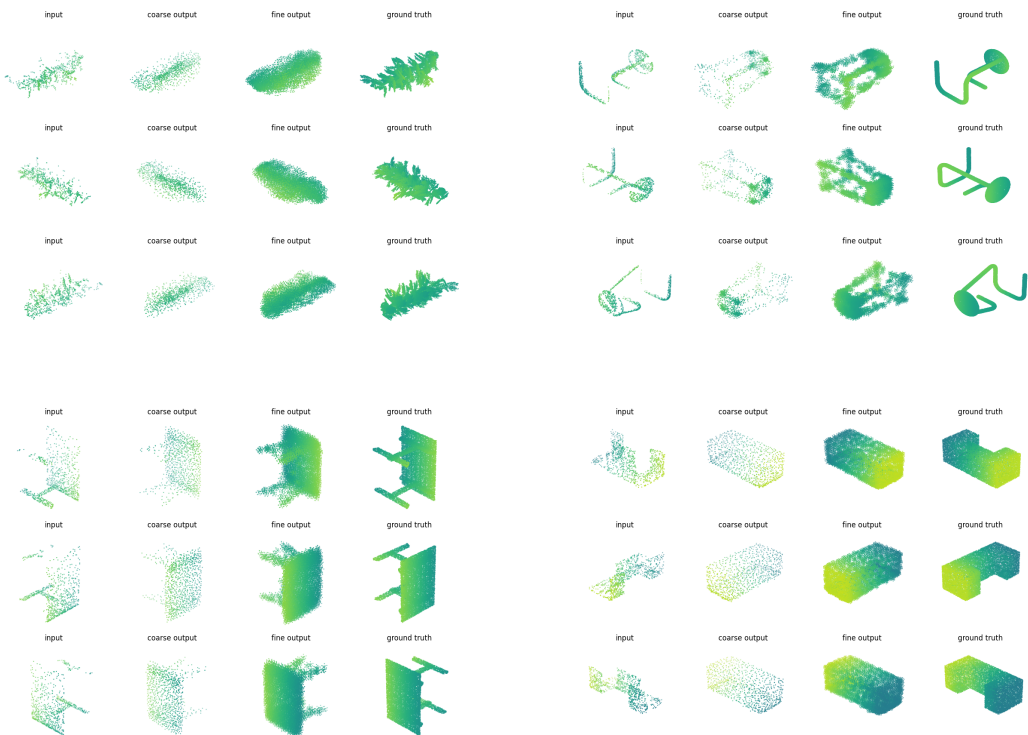


Figure 8: Failure completed examples during OcCo pre-training.

## C ANALYSIS ON THE EFFECTS OF OCCLUDED PRE-TRAINING DATASETS

We compare the occluded datasets based on ModelNet40 and ShapeNet8 for the OcCo pre-training. We construct the ModelNet Occluded using the methods described in Section 2 and for ShapeNet Occluded we directly use the data provided in the PCN, whose generation method are similar but not exactly the same with ours. Basic statistics of these two datasets are reported in Table 6.

Table 6: Statistics of occluded datasets for OcCo pre-training

Name	# of Class	# of Object	# of Views	# of Points/Object
ShapeNet Occluded (PCN)	8	30974	8	1045
ModelNet Occluded (OcCo)	40	12304	10	20085

Compared with the ShapeNet Occluded dataset which is publicized by PCN and used in all the follow-ups(Tchapmi et al., 2019; Wang et al., 2020a), our occluded ModelNet dataset has more object categories, more view-points, more points per object and therefore is more challenging. We believe such differences will help the encoder models learn a more comprehensive and robust representation which is transferable to downstream tasks. To support our idea, we perform OcCo pre-training on these two datasets respectively, and test their performance on ModelNet40 and ShapeNet Occluded classification benchmarks. The reason of choosing these two datasets for benchmarking is, ShapeNet Occluded is the out-of-domain data for the models pre-trained on ModelNet Occluded, and vice versa. We believe it will give us sufficient information on which occluded dataset should be preferred the OcCo pre-training. The Results are shown in Table 7.

Table 7: Performance of OcCo pre-trained models with different pre-trained datasets

OcCo Settings		Classification Accuracy	
Encoder	Pre-Trained Dataset	ModelNet Oc	ShapeNet Oc
PointNet	ShapeNet Oc	81.0	94.1
	ModelNet Oc	<b>85.6</b>	<b>95.0</b>
PCN	ShapeNet Oc	81.6	94.4
	ModelNet Oc	<b>85.1</b>	<b>95.1</b>
DGCNN	ShapeNet Oc	86.7	94.5
	ModelNet Oc	<b>89.1</b>	<b>95.1</b>

From Table 7, we see that the OcCo models pre-trained on ShapeNet Occluded do not perform as well as the ones pre-trained on ModelNet Occluded in most cases. Thus in our experiments, we reports the results pre-trained on ModelNet Occluded.

By visualising the objects from the ShapeNet Occluded (in Figure. 9), we believe this performance deficiency in downstream fine-training of pre-trained models is due to the quality of the generated occluded point clouds (in comparison with our generated dataset shown in Figure. 2). Further, we think our dataset is a more challenging task for all the present completion models.

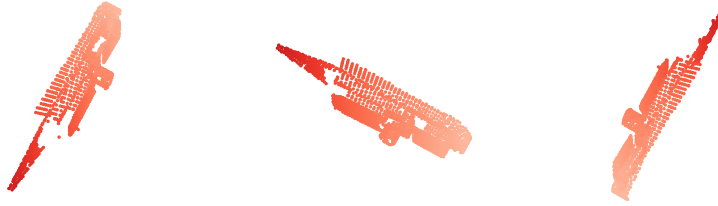
## D MORE ON SCANOBJECTNN CLASSIFICATION

In this section, we report the experimental results of random initialised and OcCo pre-trained models on all the perturbation variations of ScanObjectNNUy et al. (2019). We appreciate Ms. Mikaela Angelina Uy for granting us an early access to their data and providing helpful instructions :) We find that OcCo-initialised models are especially effective on recognising occluded point cloud objects.

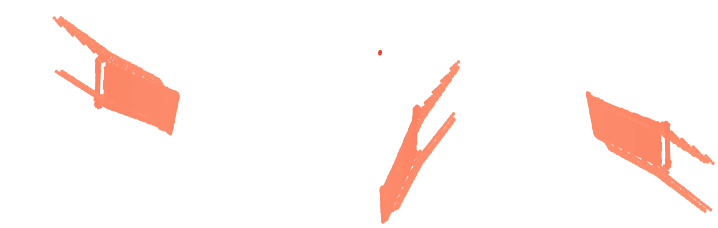
## E RE-IMPLEMENTATION DETAILS OF "JIGSAW" PRE-TRAINING METHODS

In this section, we describe how we reproduce the 'Jigsaw' pre-training methods from (Sauder & Sievers, 2019). Following their description, we first separate the objects/chopped indoor scenes into  $3^3 = 27$  small cubes and assign each point a label indicating which small cube it belongs to. We then shuffle all the small cubes, and train a model to make a prediction for each point. We reformulate this task as a 27-class semantic segmentation, for the details on the data generation and model training, please refer to our released code.

Airplane:



Chair:



Car:



Figure 9: Examples from ShapeNet Occluded which fail to depict the underlying object shapes

Table 8: Comparison of the random, Jigsaw and OcCo initialised models on all the perturbation variations of ScanObjectNN, where ‘\*’ marks the reported scores from the original literature. Note that besides ‘OBJ\_ONLY’, objects are accompanied with background points. We use the same set of terminology as in (Uy et al., 2019), ‘PB’ stands for ‘Perturbation’, ‘T\_25’ means randomly translating the object 25% along one of the xyz axis, ‘R’ represents random rotations, ‘S’ is random scaling.

Encoder	OBJ_ONLY	PB_T25	PB_T25_R	PB_T50_R	PB_T50_RS
PCN	Rand	79.3	74.4	74.8	68.3
	Jigsaw	79.2	74.9	73.8	68.5
	OcCo	<b>79.5</b>	<b>75.6</b>	<b>76.1</b>	<b>69.4</b>
PointNet	Rand*	79.2	73.5	72.7	68.2
	Jigsaw	79.1	74.6	73.6	68.2
	OcCo	<b>79.9</b>	<b>76.1</b>	<b>75.7</b>	<b>69.9</b>
DGCNN	Rand*	82.8	83.3	81.5	80.0
	Jigsaw	83.2	83.7	82.0	78.2
	OcCo	<b>84.2</b>	<b>85.0</b>	<b>83.1</b>	<b>82.8</b>

## F DETAILED RESULTS ON TRAINING A LINEAR SVM FOR CLASSIFICATION

To make a comprehensive and convincing comparison, we follow the similar procedures from (Achlioptas et al., 2018; Han et al., 2019; Sauder & Sievers, 2019; Wu et al., 2016; Yang et al., 2018), to train a linear Support Vector Machine (SVM) to examine the generalisation of OcCo encoders that are pre-trained on occluded objects from ModelNet40. For all six classification datasets, we fit a linear SVM on the output 1024-dimensional embeddings of the train split and evaluate it on the test split. **Since Sauder & Sievers (2019) have already proven their methods are better than the**

**prior, here we only systematically compare with theirs.** We report the results<sup>2</sup> in Table 9, we can see that all OcCo models achieve superior results compared to the randomly-initialized counterparts, demonstrating that OcCo pre-training helps the generalisation both in-domain and cross-domain.

Table 9: linear SVM on the output embeddings from random, Jigsaw and OcCo initialised encoders

Dataset	PointNet			PCN			DGCNN		
	Rand	Jigsaw	OcCo	Rand	Jigsaw	OcCo	Rand	Jigsaw	OcCo
ShapeNet10	91.3	91.1	<b>93.9</b>	88.5	91.8	<b>94.6</b>	90.6	91.5	<b>94.5</b>
ModelNet40	70.6	87.5	<b>88.7</b>	60.9	73.1	<b>88.0</b>	66.0	84.9	<b>89.2</b>
ShapeNet Oc	79.1	86.1	<b>91.1</b>	72.0	87.9	<b>90.5</b>	78.3	87.8	<b>91.6</b>
ModelNet Oc	65.2	70.3	<b>80.2</b>	55.3	65.6	<b>83.3</b>	60.3	72.8	<b>82.2</b>
ScanNet10	64.8	64.1	<b>67.7</b>	62.3	66.3	<b>75.5</b>	61.2	69.4	<b>71.2</b>
ScanObjectNN	45.9	55.2	<b>69.5</b>	39.9	49.7	<b>72.3</b>	43.2	59.5	<b>78.3</b>

## G MORE COMPARISONS

In Table 10, we compare OcCo with prior point-cloud-specific pre-training methods (Alliegro et al., 2020). Our method obtains the best results on all settings. These results confirm that the inductive bias learned by reconstructing occluded point clouds is stronger than one based in reconstructing permuted clouds (Alliegro et al., 2020; Sauder & Sievers, 2019). Specifically, we believe that because OcCo does not rearrange object parts but instead creates point clouds that resemble real-world 3D sensor occlusions, the initialization better encodes realistic object shape and context.

Table 10: Accuracy comparison between OcCo and prior pre-training baselines Alliegro et al. (2020) on 3D object recognition benchmarks. ModelNet40-20% means only 20% of training data are used.

Baseline	Dataset	Rand	Alliegro et al. (2020)	OcCo
PointNet	ModelNet40	89.2	89.7	<b>90.2</b>
	ModelNet40-20%	82.9	83.1	<b>83.6</b>
	ScanObjectNN (OBJ_BG)	73.7	71.3	<b>80.2</b>

## H NETWORKS AND TRAINING SETTINGS OF PCN ENCODER

We sketch the network structures of PCN encoder and output layers for downstream tasks in Figure 10.

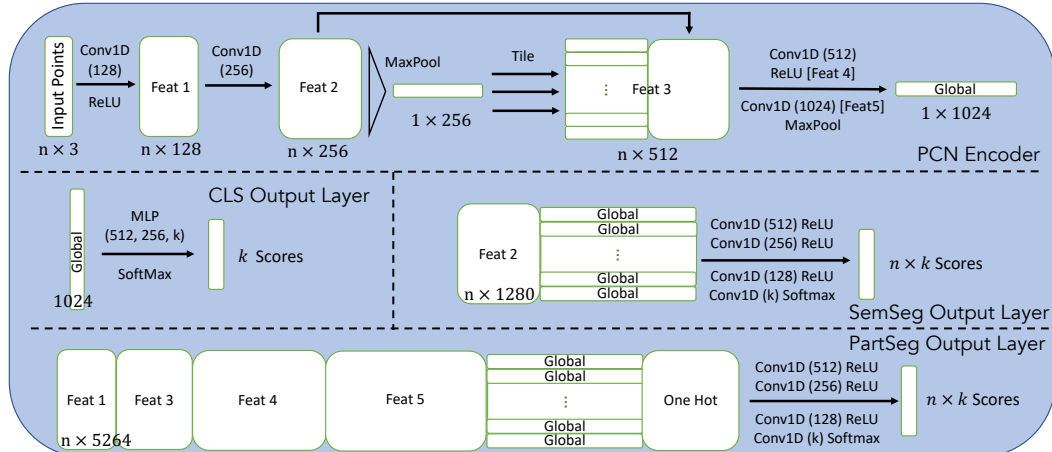


Figure 10: Encoder and Output Layers of PCN

<sup>2</sup>In our implementation, we also provide an alternative to use grid search to find the optimal set of parameters for SVM with a Radial Basis Function (RBF) kernel. In this setting, all the OcCo pre-trained models have outperformed the random initialised and Jigsaw pre-trained ones by a large margin as well.

---

## I DETAILED RESULTS OF THE PART SEGMENTATION

Here in Table 11 we report the detailed scores on each individual shape category from ShapeNetPart, we bold the best scores for each class respectively. We show that for all three encoders, OcCo-initialisation has achieved better results over two thirds of these 15 object classes.

Table 11: Detailed Results on Part Segmentation Task on ShapeNetPart

Shapes	PointNet			PCN			DGCNN		
	Rand*	Jigsaw	OcCo	Rand	Jigsaw	OcCo	Rand*	Jigsaw*	OcCo
mean (point)	83.7	83.8	84.4	82.8	82.8	83.7	85.1	85.3	<b>85.5</b>
Aero	83.4	83.0	82.9	81.5	82.1	82.4	84.2	84.1	<b>84.4</b>
Bag	78.7	79.5	77.2	72.3	74.2	79.4	83.7	<b>84.0</b>	77.5
Cap	82.5	82.4	81.7	85.5	67.8	<b>86.3</b>	84.4	85.8	83.4
Car	74.9	76.2	75.6	71.8	71.3	73.9	77.1	77.0	<b>77.9</b>
Chair	89.6	90.0	90.0	88.6	88.6	90.0	90.9	90.9	<b>91.0</b>
Earphone	73.0	69.7	74.8	69.2	69.1	68.8	78.5	<b>80.0</b>	75.2
Guitar	91.5	91.1	90.7	90.0	89.9	90.7	91.5	91.5	<b>91.6</b>
Knife	85.9	86.3	88.0	84.0	83.8	85.9	87.3	87.0	<b>88.2</b>
Lamp	80.8	80.7	81.3	78.5	78.8	80.4	82.9	83.2	<b>83.5</b>
Laptop	95.3	95.3	95.4	95.3	95.1	95.6	96.0	95.8	<b>96.1</b>
Motor	65.2	63.7	65.7	64.1	64.7	64.2	67.8	<b>71.6</b>	65.5
Mug	93.0	92.3	91.6	90.3	90.8	92.6	93.3	94.0	<b>94.4</b>
Pistol	81.2	80.8	81.0	81.0	81.5	81.5	<b>82.6</b>	<b>82.6</b>	79.6
Rocket	57.9	56.9	58.2	51.8	51.4	53.8	59.7	<b>60.0</b>	58.0
Skateboard	72.8	75.9	74.2	72.5	71.0	73.2	75.5	<b>77.9</b>	76.2
Table	80.6	80.8	81.8	81.4	81.2	81.2	82.0	81.8	<b>82.8</b>